PROCEEDINGS OF THE ROYAL SOCIETY A

Proc. R. Soc. A (2005) **461**, 671–700
doi:10.1098/rspa.2004.1371
Published online 22 December 2004

Confined developable elastic surfaces: cylinders, cones and the *Elastica*

By E. Cerda[1,2] and L. Mahadevan[2]†

[1]*Departamento de Física, Universidad de Santiago de Chile, Av. Ecuador 3493, Casilla 307, Correo 2, Santiago, Chile*
[2]*Department of Applied Mathematics and Theoretical Physics, University of Cambridge, Wilberforce Road, Cambridge CB3 0WA, UK*

We consider two of the simplest problems associated with the packing of a naturally flat thin elastic sheet. Both problems involve packing the sheet into a hollow cylinder; the first considers the partial contact of a cylindrically curved sheet with a cylindrical surface, while the second considers the partial contact of a conically curved sheet with the edge of a cylindrical surface. In each case, we solve the free-boundary problems to determine the shape, response and stability of the confined surfaces. In particular, we show that an exact description of both the cylindrical and conical structures is given by solutions of the *Elastica* equation, allowing us to present a unified description of a large class of elastic developable surfaces. This includes what is possibly the simplest example of strain localization, occurring at a point and forming one of the constituent elements of a crumpled elastic sheet.

Keywords: crumpling; packing; elastica; contact; elasticity

1. Introduction

The study of the large deformation behaviour of solid bodies is difficult, owing to the complications associated with the combined effects of geometrical and material nonlinearities. In this endeavour it is often efficacious to try to decouple those effects that arise from geometrical nonlinearities from those due to complex material behaviour. This decoupling arises naturally in the behaviour of thin elastic sheets and filaments, which can sustain large deformations while still being in the linear elastic regime, owing to the geometry-induced separation of scales. The ubiquity of these deformations scarcely requires comment: elastic sheets arise in technological problems on scales ranging from micrometres to metres, and in biology on scales from nanometres to micrometres, and surround us in the humdrum of everyday life in everything from a crumpled sheet of paper to the clothes we wear, although we are but dimly aware of the complexity associated with a quantitative description of these operations. In many of these cases, thin sheets usually can and do deform elastically and reversibly with large deflections of the order of the system size. Two observations of

† Present address: Harvard University, Cambridge, MA 02138, USA (lm@deas.harvard.edu).

Received 30 April 2003
Accepted 16 June 2004

these deformed states must be made immediately: the surface is almost never homogeneously deformed, and the surface can often have regions of self-contact where two regions initially far from each other are adjacent. The inhomogeneous deformations lead to the localization of strain and highlight a first difficulty in any treatment of these problems. In addition, contact problems involve a non-local constraint that complicates the search for solutions of the equations of elasticity which are otherwise local. Thus, despite the apparent simplicity afforded by linear elastic behaviour in these situations, there are but a few cases where analytical progress is possible; indeed these special cases are confined to planar (cylindrical) and axisymmetric deformations (Antman 1993) which do not involve the additional constraints or free boundaries associated with contact. Indeed the humble crumpled sheet that is the result of many a failed calculation is a constant reminder of the difficulties of our subject, and provides a natural generalization of packing problems, much studied in discrete geometry and statistical physics, to the realm of continuous objects such as filaments and sheets. While we are still far from understanding the complexity manifest in a crumpled sheet, in this paper we address two simple problems that allow us to understand the fundamental ingredients involved in packing a sheet. We will limit ourselves to a purely elastic analysis; this assumption would have to be abandoned in any complete study of large-scale crumpling.

We start with a reminder of the basic physics of deformation of a thin, isotropic, homogeneous, naturally flat sheet. In the long-wavelength limit considered here, the sheet has two primary modes of deformation: out-of-plane bending and in-plane stretching. Cylindrical bending into a circular arc of curvature κ preserves the middle surface of a sheet, but causes elements away from it to be strained. If the sheet has a thickness h, bending deformation produces strains of order $\gamma_{\mathrm{B}} \approx \kappa z$ at a distance z along the normal to the middle surface. The elastic energy of pure bending is then $U_{\mathrm{B}} \approx \int \mathrm{d}z\, \gamma_{\mathrm{B}}^2 \approx h^3$. On the other hand, stretching of the middle surface produces homogeneous strains through the cross-section, so that $U_{\mathrm{S}} \approx \int \mathrm{d}z\, \gamma_{\mathrm{S}}^2 \approx h$. The total energy for the elastic surface may then be written as (Rayleigh 1922)

$$\text{energy} = h^3(\text{bending}) + h(\text{stretching}). \tag{1.1}$$

Indeed, as Rayleigh and others observed more than 100 years ago,

> ... when the thickness is diminished without limit, the actual displacement will be one of pure bending, if such there be, consistent with the given conditions.
>
> (Rayleigh 1922, p. 396)

The sting in the last phrase poisons the search for a simple solution, for it refers to the importance of the boundary conditions. A sheet that is stretched clearly cannot respond by pure bending. However, one that is compressed does indeed respond by bending once the buckling threshold has been crossed. But there is another subtlety associated with arbitrary deformations. Since Gauss, we have known that isometric transformations leave the Gaussian curvature invariant. Thus, it follows that those deformations which change the Gaussian curvature cannot be isometric, and therefore must stretch the surface. Said differently, a surface which is curved in two orthogonal directions has a non-zero Gaussian curvature, and hence must be stretched. Since this is energetically prohibitively expensive, it follows that when a sheet is crumpled,

it tries to accommodate the deformations by bending in just one direction *almost everywhere*. However, owing to the nature of the constraint imposed by crumpling, namely that the sheet must be confined within a smaller volume than one that it originally inhabited, the sheet must deform by stretching in small regions leading to peaks (Mallock 1908; Ben Amar & Pomeau 1997; Cerda & Mahadevan 1998; Cerda *et al*. 1999) and ridges (Mallock 1908; Witten & Li 1993; Lobkovsky *et al*. 1995) where the deformation is highly localized. These structures act as hinges about which the whole sheet can pivot as it is crumpled and packed.

The standard approach to quantify these packing problems involves solving a set of partial differential equations that couple the bending deformations out of the plane to the stretching deformations in the plane. For a naturally flat sheet, these equations are commonly known as the Föppl–von Karman equations (Landau & Lifshitz 1997). They are only valid for small to moderate deformations, defined as those where the displacements are of the order of a few times the thickness of the sheet, but much smaller than the system size. Since this is insufficient for the large deformation problems considered here, we will eschew this approach. Instead, we start from the observation that a crumpled surface is isometric to a flat sheet almost everywhere. Differential geometry teaches us that these piecewise isometric surfaces to the plane, i.e. developable surfaces must be one of the following: perfectly flat, cylinders, cones or tangent developables (Struik 1988). Motivated by this, we will consider the simplest packing problems involving a sheet: the confinement of a circular cylindrical shell inside a rigid tube with a diameter smaller than that of the shell, and the conical confinement of a flat sheet inside a rigid conical or cylindrical container (such as a funnel). In each case, we analyse the free-boundary problems to determine the shape of the confined sheet which is in partial contact with the rigid confining boundary, and then consider its response and stability.

In § 2 we start with a description of the geometry and kinematics of deformation. In § 3, we consider constrained cylindrical deformations of sheets as our first example. This allows us to look at the two-dimensional analogue of crumpling which has one simplifying feature—the deformations are always smooth. We consider the simple packing of a cylindrical sheet into a slightly smaller cylindrical drum; the result is a region over which the sheet loses contact with the drum, leading to a free-boundary problem paradigmatic of constrained crumpling. This is analysed in terms of the classical *Elastica* of Euler, accounting for large cylindrical deformations of a sheet, or, equivalently, arbitrary planar deformations of a rod. In § 4, we focus on the case of constrained conical deformations of a sheet with a singularity at the vertex of the cone. These deformations are necessarily three dimensional, but we show that under fairly general assumptions it is possible to get an essentially exact description of these deformations using a one-dimensional equation of equilibrium. This leads to one of our main results: arbitrary large conical deformations of a sheet can also be described in terms of the classical *Elastica* using an appropriate coordinate system. In a sense, we should expect this, since conical deformations involve deformations in only one direction, i.e. one of the principal curvatures of the sheet vanishes. In terms of the *Elastica* we then consider the conical packing of a sheet that is forced into a cylinder frame (Cerda & Mahadevan 1998; Cerda *et al*. 1999) and analyse the resulting free-boundary problem for the so-called conical dislocation that is one of the main ingredients of crumpled sheet. Finally, in § 5 we close with a discussion of

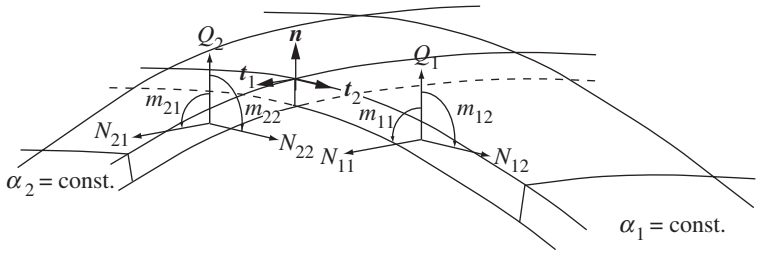

Figure 1. Components of the forces N_{ij}, Q_{ij} and moments m_{ij} along the oriented sections defined by the coordinate curves $\alpha_2 = \text{const.}$ and $\alpha_1 = \text{const.}$

how our approach may be used as a possible means of unravelling the complexity of crumpled continua.

2. Geometrical and mechanical description of an inextensible surface

The middle surface of an inextensible sheet preserves its length in any direction. In differential geometry this is equivalent to the statement that its first fundamental form is invariant under this class of deformations. More precisely, if the surface is described by the parametrization $\boldsymbol{r}(\alpha_1, \alpha_2)$, with α_1 and α_2 being the Lagrangian coordinates of a material point of the middle surface, the metric tensor

$$g_{ij} = \partial_{\alpha_i} \boldsymbol{r} \cdot \partial_{\alpha_j} \boldsymbol{r}, \quad i, j = 1, 2, \tag{2.1}$$

is constant. It follows that any geometrical quantity which is a function only of the metric tensor will be an invariant of the deformation. One of the most famous examples of such a quantity is embodied in Gauss's 'Theorema Egregium' (Kreyszig 1991; Struik 1988); since the Gaussian curvature can be expressed purely in terms of the metric tensor, it is also an invariant of inextensible surfaces. Thus, if a naturally flat surface with zero Gaussian curvature is deformed inextensibly, its final state will also have zero Gaussian curvature. Then, the curvature in at least one of the principal directions at every point is always zero. Assuming that the deformations are continuous and differentiable, this leads to the conclusion that through every point one of the lines of curvature is a straight line. These lines are called generators, and a visualization of their presence is afforded in a bent transparency in ambient light which reflects strongly off the straight generators.

For any such an isometric deformation, we must augment the previous geometrical description with a statement about the equilibrium of forces and moments to describe a physical sheet. We will denote the tangent to the line $\alpha_2 = \text{const.}$ as $\boldsymbol{t}_1$, the tangent to the line $\alpha_1 = \text{const.}$ as $\boldsymbol{t}_2$ and the normal to the surface as $\boldsymbol{n}$, i.e. $(\partial_{\alpha_i} = \partial/\partial\alpha_i)$:

$$\boldsymbol{t}_1 = \frac{\partial_{\alpha_1} \boldsymbol{r}}{g_{11}^{1/2}}, \qquad \boldsymbol{t}_2 = \frac{\partial_{\alpha_2} \boldsymbol{r}}{g_{22}^{1/2}}, \qquad \boldsymbol{n} = \boldsymbol{t}_1 \times \boldsymbol{t}_2. \tag{2.2}$$

Here $\alpha_2 = \text{const.}$ and $\alpha_1 = \text{const.}$ define a local orthogonal coordinate system.

Consider the force per unit length at a cross-section defined by the curvilinear coordinate $\alpha_2 = \text{const.}$ Since the normal to the cross-section lies along $\boldsymbol{t}_2$, we denote the force $\boldsymbol{F}_2$, following the convention introduced by Reissner (1941). This force can be resolved into its orthogonal components (see figure 1)

$$\boldsymbol{F}_2 = N_{21}\boldsymbol{t}_1 + N_{22}\boldsymbol{t}_2 + Q_2\boldsymbol{n}. \tag{2.3}$$

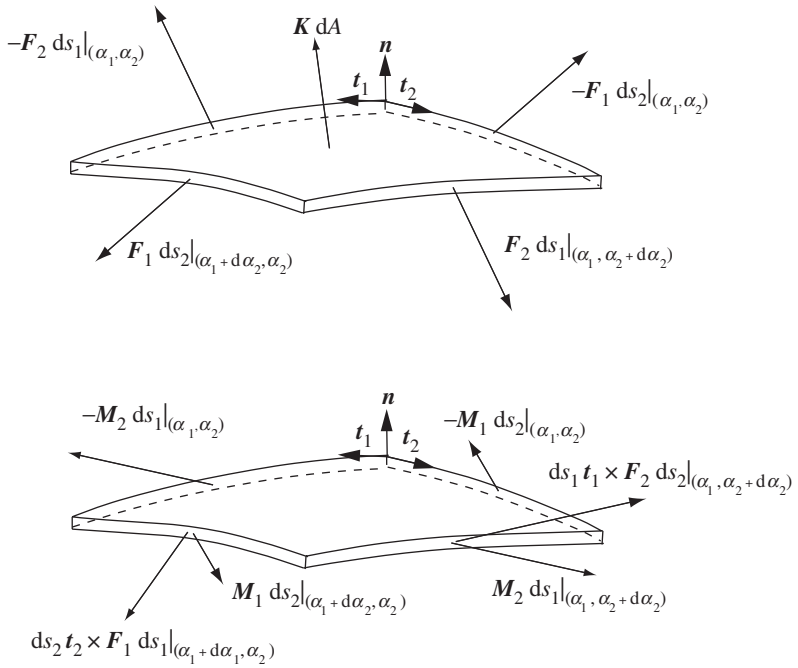

Figure 2. Forces $\boldsymbol{F}$ and moments $\boldsymbol{M}$ on an infinitesimal segment defined by the intersection of the coordinate curves $\alpha_1 = \text{const.}$, $\alpha_2 = \text{const.}$, $\alpha_1 + \mathrm{d}\alpha_1 = \text{const.}$ and $\alpha_2 + \mathrm{d}\alpha_2 = \text{const.}$

Similarly, the force per unit length at a cross-section defined by the coordinate $\alpha_1 = \text{const.}$ is

$$\boldsymbol{F}_1 = N_{11}\boldsymbol{t}_1 + N_{12}\boldsymbol{t}_2 + Q_1\boldsymbol{n}. \tag{2.4}$$

Here N_{11}, N_{22} are the in-plane tensile stress resultants, while N_{12}, N_{21} are the in-plane shear resultants, and Q_1, Q_2 are the out-of-plane stress resultants. In general, $N_{12} \neq N_{21}$ since they correspond to forces on different elemental areas. If in addition, we denote the force per unit area as $\boldsymbol{K}$, the equations of force equilibrium deduced from figure 2 lead to

$$\begin{aligned}-\boldsymbol{F}_2\,\mathrm{d}s_1|_{(\alpha_1,\alpha_2)} + \boldsymbol{F}_2\,\mathrm{d}s_1|_{(\alpha_1,\alpha_2+\mathrm{d}\alpha_2)}\\ - \boldsymbol{F}_1\,\mathrm{d}s_2|_{(\alpha_1,\alpha_2)} + \boldsymbol{F}_1\,\mathrm{d}s_2|_{(\alpha_1+\mathrm{d}\alpha_1,\alpha_2)} + \boldsymbol{K}|_{(\alpha_1,\alpha_2)}\,\mathrm{d}A = 0.\end{aligned} \tag{2.5}$$

Here $\mathrm{d}s_1 = A_1\,\mathrm{d}\alpha_1$ is the arc length in the $\boldsymbol{t}_1$-direction and $A_1 = g_{11}^{1/2}$. Similarly, $\mathrm{d}s_2 = A_2\,\mathrm{d}\alpha_2$, where $A_2 = g_{22}^{1/2}$, and $\mathrm{d}A$ is the element of area:

$$\mathrm{d}A = (\det g)^{1/2}\,\mathrm{d}\alpha_1\,\mathrm{d}\alpha_2 = A_1A_2\,\mathrm{d}\alpha_1\,\mathrm{d}\alpha_2.$$

Next, we define $\boldsymbol{M}_2$ as the couple per unit of length of the middle surface parametrized by the coordinate $\alpha_2 = \text{const.}$ Since it is generated by a variation of the stress in the $\boldsymbol{n}$-direction, it may be written as (see figure 1)

$$\boldsymbol{M}_2 = \boldsymbol{n}\times(m_{21}\boldsymbol{t}_1 + m_{22}\boldsymbol{t}_2). \tag{2.6}$$

Here m_{11}, m_{22} are the bending torque resultants, while m_{12}, m_{21} are the twisting torque resultants. Similarly, we define $\boldsymbol{M}_1$ as the couple per unit of length of the middle surface parametrized by the coordinate $\alpha_1 = \text{const.}$ Resolving it into components,

we write

$$\boldsymbol{M}_1 = \boldsymbol{n} \times (m_{11}\boldsymbol{t}_1 + m_{12}\boldsymbol{t}_2). \tag{2.7}$$

The balance of torques may then be deduced from figure 2 and leads to

$$\begin{aligned} &- \boldsymbol{M}_2\, \mathrm{d}s_1|_{(\alpha_1,\alpha_2)} + \boldsymbol{M}_2\, \mathrm{d}s_1|_{(\alpha_1,\alpha_2+\mathrm{d}\alpha_2)} - \boldsymbol{M}_1\, \mathrm{d}s_2|_{(\alpha_1,\alpha_2)} \\ &\quad + \boldsymbol{M}_1\, \mathrm{d}s_2|_{(\alpha_1+\mathrm{d}\alpha_1,\alpha_2)} \mathrm{d}s_2 \boldsymbol{t}_2 \times \boldsymbol{F}_2\, \mathrm{d}s_1|_{(\alpha_1,\alpha_2+\mathrm{d}\alpha_2)} + \mathrm{d}s_1 \boldsymbol{t}_1 \times \boldsymbol{F}_1\, \mathrm{d}s_2|_{(\alpha_1+\mathrm{d}\alpha_1,\alpha_2)} = \boldsymbol{0}. \end{aligned} \tag{2.8}$$

Rewriting equations (2.5) and (2.8) to reflect the local equations of force and torque equilibrium yields

$$\left.\begin{aligned} \partial_{\alpha_1}(A_2\boldsymbol{F}_1) + \partial_{\alpha_2}(A_1\boldsymbol{F}_2) + A_1A_2\boldsymbol{K} = \boldsymbol{0}, \\ \partial_{\alpha_1}(A_2\boldsymbol{M}_1) + \partial_{\alpha_2}(A_1\boldsymbol{M}_2) + A_1A_2(\boldsymbol{t}_1 \times \boldsymbol{F}_1 + \boldsymbol{t}_2 \times \boldsymbol{F}_2) = \boldsymbol{0}. \end{aligned}\right\} \tag{2.9}$$

Then (2.9) constitutes a set of six differential equations for the ten unknowns corresponding to the six force and four torque components at any point on the middle surface of the sheet. To close the system, we need some constitutive relations that relate to the physical response of the material of the sheet.

Towards this end, we recall the fundamental theorem in the differential geometry of surfaces which states that the first and second fundamental forms of a surface completely define it up to rigid-body motions (Struik 1988). The first fundamental form is a scalar defined in terms of the components of the metric tensor g_{ij}, while the components of the second fundamental form can similarly be defined in terms of the curvature tensor

$$b_{ij} = -\boldsymbol{n} \cdot \partial_{\alpha_i}\partial_{\alpha_j}\boldsymbol{r}. \tag{2.10}$$

In terms of the coefficients of the curvature and metric tensors, we can define $\kappa_1 = b_{11}/g_{11}$ as the normal curvature along $\boldsymbol{t}_1$, $\kappa_2 = b_{22}/g_{22}$ as the normal curvature along the $\boldsymbol{t}_2$-direction, and $\tau = b_{12}/(g_{11}g_{22})^{1/2}$ as the geodesic torsion or twist of the surface.

We pause to consider our sign convention, which is consistent with that of classical shell theory (Reissner 1941; Dym 1990) but different from that of classical differential geometry (Kreyszig 1991; Struik 1988). Couples are considered positive when they have the same sign as couples resulting from positive stresses on the part of the shell above the middle surface, where above and below is defined by the orientation of the normal. Furthermore, we define a positive curvature when the centre of curvature is below the middle surface and a positive twist when the lines $\alpha_1 = \text{const.}$ rotate clockwise about the axis defined by $\boldsymbol{t}_1$.

When the surface is deformed inextensibly, the first fundamental form is preserved but the second fundamental form (and therefore the curvature) varies. At the lowest order the constitutive relations relating the couples and curvatures for a naturally flat sheet are (Love 1944; Dym 1990)

$$m_{11} = B(\kappa_1 + \sigma\kappa_2), \qquad m_{22} = B(\kappa_2 + \sigma\kappa_1), \qquad m_{12} = m_{21} = B(1-\sigma)\tau, \tag{2.11}$$

where σ is Poisson's ratio of the material of the sheet, $B = Eh^3/12(1-\sigma^2)$ is the bending stiffness and E is the Young modulus of the sheet. At this order of approximation the couples $m_{12} = m_{21}$ but it is not true generally for thick shells; higher-order constitutive relations can be found in Love (1944, pp. 565).

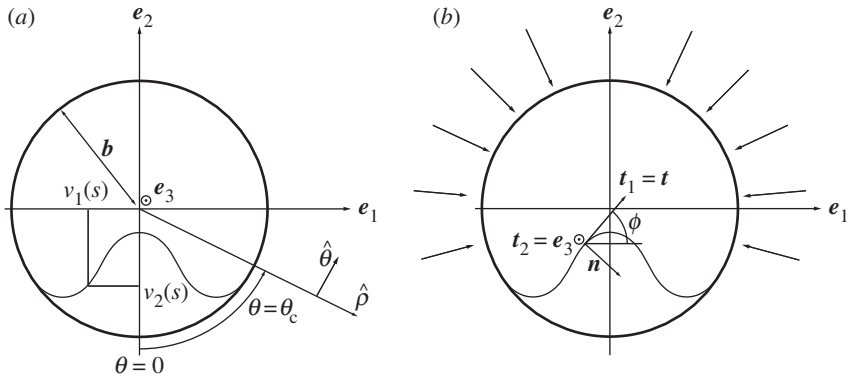

Figure 3. Schematic of a puckered cylinder. (*a*) Puckering of a cylindrical surface of radius R into another of smaller radius b. The puckering can be described by using a two-dimensional geometry, so that the deformation is given by the vector $\boldsymbol{v}(s) = (v_1(s), v_2(s))$. (*b*) Definition of the trihedron $\{\boldsymbol{t}_1, \boldsymbol{t}_2, \boldsymbol{n}\}$.

To complete the formulation of the problem, we note that the curvature and metric tensors must satisfy a set of compatibility relations known as the Gauss–Codazzi relations, which are (Kreyszig 1991; Struik 1988)

$$\left.\begin{aligned} \partial_{\alpha_2} b_{11} - \partial_{\alpha_1} b_{12} &= b_{11}\Gamma^1_{12} + b_{12}(\Gamma^2_{22} - \Gamma^1_{11}) - b_{22}\Gamma^2_{11}, \\ \partial_{\alpha_2} b_{12} - \partial_{\alpha_1} b_{22} &= b_{11}\Gamma^1_{22} + b_{12}(\Gamma^2_{22} - \Gamma^1_{12}) - b_{22}\Gamma^2_{12}, \\ \frac{\det g}{\det b} &= \frac{1}{\det g}\left(\partial_{\alpha_1}\left(\frac{\det g\Gamma^1_{22}}{g_{22}}\right) - \partial_{\alpha_2}\left(\frac{\det g\Gamma^1_{12}}{g_{22}}\right)\right), \end{aligned}\right\} \tag{2.12}$$

where $\Gamma^k_{ij} = \partial_{\alpha_i}\partial_{\alpha_j}\boldsymbol{r} \cdot \partial_{\alpha_k}\boldsymbol{r}$ are the Christoffel symbols which may be expressed purely in terms of the components of the metric tensor, i.e. they are invariant for isometric deformations.

Substituting the relations (2.11) into (2.9) leads to the elimination of the moments in favour of the components of the first and second fundamental forms b_{ij}, g_{ij}. Since we are interested in inextensible deformations, g_{ij} are invariant. Then, the determination of the shape of the surface and the forces on it requires that we determine the three coefficients of the second fundamental form b_{ij} and the six unknown forces N_{11}, N_{22}, N_{12}, N_{21}, Q_1, Q_2, i.e. a total of nine unknowns. And we have exactly the right number of equations: the six equations of equilibrium (2.9) and the three relations of Gauss–Codazzi (2.12). Of course, these equations must be supplemented by appropriate boundary condition on some combination of the stress and couple resultants and/or the displacements. In the following sections we will consider two concrete examples that apply the preceding equations to the packing of a naturally flat sheet into a slightly smaller cylindrical drum via either cylindrically or conically deformed sheets.

3. The puckered cylinder

(*a*) *Geometry*

We consider a very long sheet rolled into the shape of a circular cylinder of radius R. The lateral ends of the sheet are glued to each other, and the resulting long cylindrical

sheet is then introduced into a cylinder of radius $b < R$ as shown in figure 3. The excess length of the sheet causes it to pucker with a natural dimensionless control parameter to describe the packing in this system given by

$$\varepsilon^2 = \frac{(R-b)}{b}. \tag{3.1}$$

Assuming that the deformation of the sheet is cylindrical, the position vector describing the sheet can be written as

$$\boldsymbol{r}(s,z) = \boldsymbol{v}(s) + z\boldsymbol{e}_3, \tag{3.2}$$

where $\boldsymbol{v}(s) = v_1(s)\boldsymbol{e}_1 + v_2(s)\boldsymbol{e}_2$, s is the arc length of the two-dimensional curve defined by $\boldsymbol{v}(s)$ and z is the length along the axis of the cylinder (see figure 3*a*). We observe that this class of one-dimensional deformations automatically satisfies the Gauss–Codazzi relations (2.12).

The metric tensor associated with this deformation is $g_{ss} = 1$, $g_{sz} = 0$, $g_{zz} = 1$, and the orthonormal vector triad describing the surface is

$$\boldsymbol{t}_1 = \boldsymbol{t}, \qquad \boldsymbol{t}_2 = \boldsymbol{e}_3, \qquad \boldsymbol{n} = \boldsymbol{t} \times \boldsymbol{e}_3. \tag{3.3}$$

Here $\boldsymbol{t} = \partial_s \boldsymbol{v}$ is the tangent and $\boldsymbol{n}$ is the oriented normal to the planar curve that completely describes the cylindrical sheet. In terms of the angle ϕ between $\boldsymbol{t}$ and the horizontal (figure 3*b*), we have $\boldsymbol{t} = \cos\phi\boldsymbol{e}_1 + \sin\phi\boldsymbol{e}_2$ and $\boldsymbol{n} = \sin\phi\boldsymbol{e}_1 - \cos\phi\boldsymbol{e}_2$. The components of the curvature tensor are given by $b_{ss} = \kappa$, $b_{zz} = b_{sz} = 0$, where $\kappa = -\boldsymbol{n}\cdot\partial_s\boldsymbol{t} = \dot{\phi}$ is the curvature of the planar curve shown in figure 3. Here and elsewhere, we use the notation $\dot{(\cdot)} \equiv \partial_s(\cdot)$. The lines $z =$ const. and $s =$ const. are the lines of curvature for all possible deformations, so that the geodesic torsion $\tau = 0$ identically. Therefore, $m_{sz} = m_{zs} = 0$. Since the normal curvature along the line $s =$ const. is zero, $m_{ss} = B\kappa$, $m_{zz} = B\sigma\kappa$. Finally, torque equilibrium in the $\boldsymbol{n}$-direction yields $N_{sz} = N_{zs}$. Here we see an example where the local torques and forces are symmetric.

(*b*) *Mechanical equilibrium*

In the absence of any frictional interactions with the confining cylinder the external force must be along the normal so that $\boldsymbol{K} = -k\boldsymbol{n}$ ($k > 0$). For a very long cylinder, we may safely neglect any variations along the axial direction $\boldsymbol{e}_3$, so that $\partial(\cdot)/\partial z = 0$ in (2.9). Then, we need to consider just the projection of the equations of force and torque equilibrium on a plane perpendicular to the cylinder axis:†

$$\left.\begin{aligned} \partial_s\boldsymbol{F} + \boldsymbol{K} &= \boldsymbol{0},\\ \partial_s\boldsymbol{M} + \boldsymbol{t}\times\boldsymbol{F} &= \boldsymbol{0}. \end{aligned}\right\} \tag{3.4}$$

Here the local force resultant at a cross-section is $\boldsymbol{F} = N_{ss}\boldsymbol{t} + Q_s\boldsymbol{n}$ and the torque resultant is $\boldsymbol{M} = m_{ss}\boldsymbol{n}\times\boldsymbol{t} = B\kappa\boldsymbol{e}_3$. The equations (3.4) then correspond to those for the equilibrium of elastic rods and their analysis is now classical (Landau & Lifshitz 1997).

† The other components of the forces and couples can be determined by using the remaining equations, but they will be sensitive to the forces and couples applied at the lateral ends of the cylinder.

(*c*) *Global force balance*

Writing out the equilibrium equations (3.4) in component form yields the relations

$$\partial_s N_{ss} + \kappa Q_s = 0, \tag{3.5}$$

$$\partial_s Q_s - \kappa N_{ss} = k(s), \tag{3.6}$$

$$B\dot{\kappa} = Q_s. \tag{3.7}$$

The first two correspond to force balance in the tangential and normal directions, while the last equation is a consequence of torque equilibrium. By using the relation (3.7) in (3.5) we can integrate it once so that $N_{ss} + B\kappa^2/2 = -Ba^2$, where a^2 is a constant of integration. Substituting the result in equation (3.6) yields

$$B[\ddot{\kappa} + (a^2 + \tfrac{1}{2}\kappa^2)\kappa] = k(s), \tag{3.8}$$

which, together with appropriate boundary conditions, describes the equilibrium shape of the *Elastica* of Euler. For the confined cylindrical sheet shown in figure 3, the radius of curvature is constant and equal to the radius of the external cylinder $\kappa = 1/b$ in the region where the sheet is in contact with the rigid cylinder. Therefore, it follows from (3.8) that $k = k_{\mathrm{c}} = \text{const.}$ in this region. Furthermore, in the contact region $\dot{\kappa} = 0$ so that (3.7) implies $Q_s = 0$ and (3.6) implies $N_{ss} = -bk_{\mathrm{c}}$, i.e. the sheet is under purely normal compression due to confinement.

To characterize the free region, we define $s = 0$ as the generator at the centre of the fold. Solving (3.8) with $k(s) = 0$ by looking for an even function of the arc length s yields

$$\kappa = \kappa_1 \,\mathrm{cn}((a^2 + \tfrac{1}{2}\kappa_1^2)^{1/2} s \mid m), \tag{3.9}$$

where κ_1 is the curvature at $s = 0$ and $m = \kappa_1^2/(4a^2 + 2\kappa_1^2)$ is the modulus of the cnoidal Jacobi elliptic function, $\mathrm{cn}(\cdot \mid \cdot)$.

To determine the forces along the contact line, we consider the conditions imposed by global force balance. The total force on the right half of the cylinder is given by

$$\boldsymbol{W}_{\mathrm{right}} = \int_{s_{\mathrm{c}}}^{\pi R} \mathrm{d}s(-k_{\mathrm{c}}\boldsymbol{n}), \tag{3.10}$$

where s_{c} is the arc length at the contact line measured from the intersection of the sheet with the axis of symmetry. Since $\phi = \theta$ the polar angle and $\dot{\theta} = 1/b$ for $s_{\mathrm{c}} < s < \pi$, we get

$$\boldsymbol{W}_{\mathrm{right}} = -bk_{\mathrm{c}}((1 + \cos\theta_{\mathrm{c}})\boldsymbol{e}_1 + \sin\theta_{\mathrm{c}}\boldsymbol{e}_2), \tag{3.11}$$

where $\theta_{\mathrm{c}} = \theta(s_{\mathrm{c}})$. Similarly the force applied on the left half of the cylinder can be readily obtained as

$$\boldsymbol{W}_{\mathrm{left}} = -bk_{\mathrm{c}}(-(1 + \cos\theta_{\mathrm{c}})\boldsymbol{e}_1 + \sin\theta_{\mathrm{c}}\boldsymbol{e}_2).$$

We see that there is an unbalanced external force of magnitude $-bk_{\mathrm{c}}\sin\theta_{\mathrm{c}}$ on each half that acts along the plane of symmetry. To satisfy force equilibrium, localized forces must be applied at the contact lines to balance the force from the rest of sheet, i.e. we must have

$$\int_{s_{\mathrm{c}}^-}^{s_{\mathrm{c}}^+} \mathrm{d}s\, \boldsymbol{e}_2 \cdot \boldsymbol{K}_{\mathrm{l}} - bk_{\mathrm{c}}\sin\theta_{\mathrm{c}} = 0, \tag{3.12}$$

where $s_c^{\pm} = s_c \pm \eta$, $\eta \to 0$, and $\boldsymbol{K}_1$ is the localized contribution to the body force in the neighbourhood of the contact point. Letting $\boldsymbol{K}_1 = -\chi\delta(s - s_c)\boldsymbol{n}$, we get $\chi = bk_c \tan\theta_c$. The total body force $\boldsymbol{K}$ is the sum of the uniform normal pressure over the contact zone and the localized force along the contact line i.e.

$$\boldsymbol{K} = -k_c(1 + b\tan\theta_c\delta(|s| - s_c))\boldsymbol{n}, \quad |s| \geqslant s_c. \tag{3.13}$$

Here the form of $\boldsymbol{K}$ is dictated by symmetry. The localized external forces produce a discontinuity in the internal shear forces in the sheet at the contact line. We can see this by integrating the first equation in (3.4) in the neighbourhood of the contact line, so that

$$\boldsymbol{F}_+ - \boldsymbol{F}_- + \int_{s_c^-}^{s_c^+} \mathrm{d}s\, \boldsymbol{K} = 0, \tag{3.14}$$

where $\boldsymbol{F}_\pm = \boldsymbol{F}(s_c \pm \eta)$. Using the expression for $\boldsymbol{K}$ from (3.13) in (3.14), we find that the force in the free region is $\boldsymbol{F} = -(bk_c/\cos\theta_c)\boldsymbol{e}_1$. Therefore, for the entire sheet we may write

$$\boldsymbol{F} = \begin{cases} -bk_c\boldsymbol{t} & \text{if } |s| > s_c, \\ -\dfrac{bk_c}{\cos\theta_c}\boldsymbol{e}_1 & \text{if } |s| < s_c. \end{cases}$$

(*d*) *Small-deflection analysis*

We now turn to the determination of the unknown parameters k_c, s_c and θ_c which determine the contact forces and the location of the free boundaries. The excess length of the sheet relates s_c and θ_c via the equation

$$s_c - b\theta_c = \pi(R - b) = \pi b\varepsilon^2. \tag{3.15}$$

The continuity of ϕ and the curvature $\dot{\phi}$ across the contact line which follow by integrating the equation of equilibrium (3.8) yield $\phi(s_c) = \theta_c$ and $\dot{\phi}(s_c) = 1/b$, i.e.

$$\int_0^{s_c} \mathrm{d}s\, \kappa = \theta_c, \tag{3.16}$$

$$\kappa(s_c) = \frac{1}{b}. \tag{3.17}$$

The condition that the sheet, and therefore the curve which is its projection onto a plane perpendicular to its axis, is closed requires that the total projection of the curve along the $\boldsymbol{e}_1$ is zero. Because $\dot{v}_1 = \cos\phi$, we can write this condition as

$$\int_0^{\pi R} \mathrm{d}s\, \cos\phi = 0. \tag{3.18}$$

Finally, evaluating (3.8) away from the point $s = s_c$ yields an expression for the dimensionless confining force:

$$(ba)^2 + \tfrac{1}{2} = \frac{b^3 k_c}{B}. \tag{3.19}$$

Before solving the system (3.8), (3.15)–(3.19) for the geometry of the puckered cylinder, we provide a scaling analysis of this system when $\varepsilon \ll 1$, $\theta_c \ll 1$. Then the

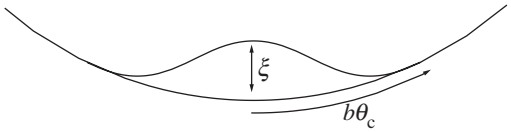

Figure 4. Geometry of the fold. The inextensibility constraint yields $\sqrt{\xi^2 + (b\theta_c)^2} - b\theta_c \sim \pi b\varepsilon^2$ for the excess of length.

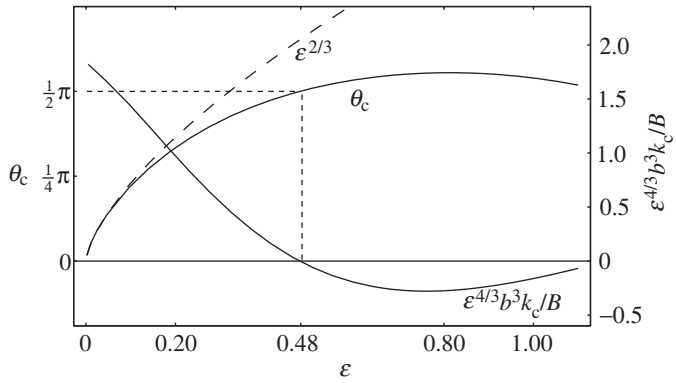

Figure 5. The position of the contact angle θ_c and the dimensionless external force $\varepsilon^{4/3}b^3k_c/B$ as a function of the packing parameter ε. For $\varepsilon \geqslant 0.48$, $b^3k_c/B < 0$, i.e. the external force must be adhesive to prevent the collapse of the structure.

vertical displacement of the fold ξ (see figure 4) and the excess length s_c given by (3.15) are then related by the geometrical equation

$$\begin{aligned} s_c - b\theta_c &\approx \sqrt{\xi^2 + (b\theta_c)^2} - b\theta_c \\ &\approx \frac{\xi^2}{b\theta_c}. \end{aligned} \tag{3.20}$$

Comparing (3.15) with (3.20), we find that $\xi^2/b\theta_c \approx b\varepsilon^2$. Furthermore, since the curvature of the fold in the vicinity of the contact point $\kappa \approx \xi/(b\theta_c)^2$ must be the curvature of the confining cylinder, we have $\xi/(b\theta_c)^2 \approx 1/b$. From these two relations we find scaling laws for the displacement $\xi \approx b\varepsilon^{4/3}$, the contact angle $\theta_c \approx \varepsilon^{2/3}$ and the arc length of the fold $s_c \approx b\theta_c \approx b\varepsilon^{2/3}$.

To estimate the internal forces, we consider moments about the position $s = 0$. The internal moment $M \approx B/b$ must be balanced by the torque due to the reaction forces at the contact point $M \approx bk_c\xi$. Therefore, the dimensionless compressive force due to the confining cylinder scales as

$$\frac{b^3k_c}{B} \approx \frac{b}{\xi} \approx \varepsilon^{-4/3}. \tag{3.21}$$

We see that as $\varepsilon \to 0$, the required compressive stress to stabilize the fold diverges. This divergence is cut-off when the size of the fold becomes comparable to the thickness of the sheet, as our simple one-dimensional theory accounting for bending alone is not valid in this limit.

(e) *Large-deflection analysis*

To corroborate our scaling analyses and extend our results to the case when the packing parameter ε is not small, we solve the system (3.8), (3.15)–(3.19) numerically. In figure 5 we show the dependence of θ_c and $b^3 k_c/B$ on ε and see that our scaling estimates from the previous section are valid when $\varepsilon \ll 1$. However, as ε becomes larger, we see that the dimensionless force $b^3 k_c/B$ decreases and eventually vanishes when $\varepsilon \approx 0.48$. Thus the sheet needs adhesive forces to guarantee equilibrium when $\varepsilon \geqslant 0.48$ and suggests that the system with a single symmetric fold is unstable when $\varepsilon \geqslant 0.48$. The mechanism of the instability becomes obvious when we notice that $\theta_c = \pi/2$ for $\varepsilon \approx 0.48$, i.e. it is impossible to balance forces in the $\boldsymbol{e}_2$-direction by using only localized external forces along the lines of contact. Thus, we expect to see the development of possibly asymmetric folds to stabilize the system beyond this point, a subject worthy of study but one that we shall not pursue here.

4. The puckered cone

The three-dimensional analogue of packing a planar curve into a circle (or equivalently of packing a cylindrically deformed sheet into a slightly smaller cylinder as treated in the previous section) is the packing of a sheet into a sphere. However, the latter problem is far more difficult than one might first imagine owing to the strong constraints imposed by geometry and the contact conditions. Here we will consider the somewhat simpler situation of packing a sheet into an open cylindrical frame which can be achieved via a conically deformed shape much like a coffee filter paper as depicted in figure 6*a*, a geometry first studied nearly a century ago by Mallock (1908), who pointed out the importance of inextensible conical deformations. More recently (Cerda & Mahadevan 1998; Cerda *et al*. 1999) we showed that this geometry is amenable to analysis and experiment. Here, we revisit this problem and show that it is possible to reduce the fully nonlinear problem to quadratures allowing us to examine the solutions in some detail.

(a) *Geometry*

When a circular sheet of paper of radius R_p is pushed into a cylindrical frame of radius R by applying a centred transverse force directed along the axis of the cylinder, as shown in figure 6*a*, it responds by buckling out of the plane to form a non-axisymmetric conical surface that is only in partial contact with the frame. The effectiveness of packing is controlled by the axial distance d through which the tip is pushed into the frame, and defines a dimensionless packing parameter $\varepsilon = d/R$. Geometrically, the surface may be described by a family of generators originating at the centre of the sheet, with the angle β between a generator and the vector $\boldsymbol{e}_3$ characterizing the normal to the plane of the supporting frame. When

$$\cot \beta_c = \varepsilon \tag{4.1}$$

the generators are in contact with the frame and the shape of the sheet is a cone of opening angle β_c.† Of course, this conical shape only describes part of the sheet,

† In the following all the variables evaluated along the contact region will carry the subscript 'c'.

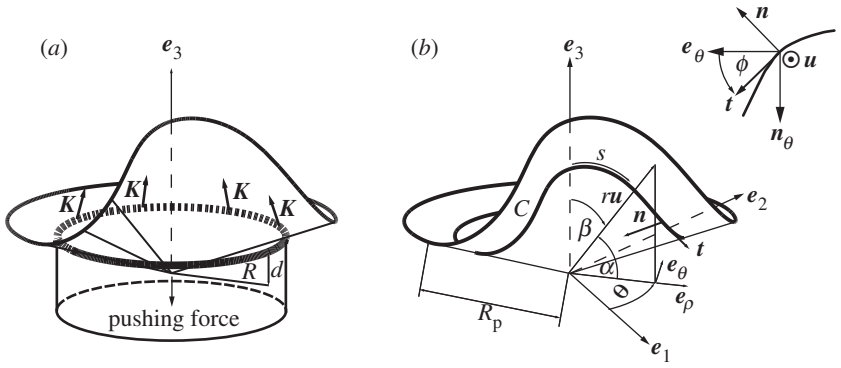

Figure 6. Schematic of a puckered cone. (*a*) An axial force at the centre of the plate makes it buckle into a conical shape with one fold. The normal forces $\boldsymbol{K}$ act along the line of contact between the cone and the cylindrical frame. (*b*) The angles θ and β with respect to an Eulerian frame and the moving orthonormal trihedron $\{\boldsymbol{t}, \boldsymbol{u}, \boldsymbol{n}\}$ characterize the surface.

since all the generators cannot satisfy (4.1) without violating the inextensibility condition. The non-axisymmetric conical shape shown in figure 6*a* is therefore a natural outcome of respecting the constraint of inextensibility almost everywhere, except in the vicinity of the tip. In addition to forming a simple system in which to study the packing problem of a sheet, this example thus affords the simplest example of stress, strain and energy localization occurring in the vicinity of a point, namely the centre of the sheet.

The most general description of a conical shape is given by the parametrization

$$\boldsymbol{r}(s, r) = r\boldsymbol{u}(s), \tag{4.2}$$

where r is the distance from the origin located at the tip, $\boldsymbol{u}(s)$ is a unit vector, and s is the arc length of the curve (see figure 6*b*) measured from the position of maximum elevation of the fold. The motion of $\boldsymbol{u}(s)$ describes a curve $\mathcal{C}$ in space. Since the total length of this curve surrounding the tip is invariant under inextensible deformations, a circular curve with initial length 2π (at an initial radius $r = 1$) will not change its length. Therefore, the surface defined by the locus of the straight line $r\boldsymbol{u}(s)$ will be a developable surface. The metric tensor associated with this class of deformations has components $g_{ss} = r^2$, $g_{sr} = 0$ and $g_{rr} = 1$ and remains constant. To describe the surface, we use a moving orthonormal trihedron (equivalent to the *repère mobile* of Cartan)

$$\boldsymbol{t}_1 = \boldsymbol{t}, \qquad \boldsymbol{t}_2 = \boldsymbol{u}, \qquad \boldsymbol{n} = \boldsymbol{t} \times \boldsymbol{u}. \tag{4.3}$$

Here $\boldsymbol{t}$ is the tangent vector to the curve $\mathcal{C}$, and $\boldsymbol{t}$ and $\boldsymbol{n}$ are in a plane perpendicular to $\boldsymbol{u}$. To parametrize the vectors $\boldsymbol{t}$, $\boldsymbol{u}$, $\boldsymbol{n}$ while emphasizing the correspondence with the packing problem treated in § 3, we use the vectors $\boldsymbol{e}_\theta$ and $\boldsymbol{n}_\theta = \boldsymbol{u} \times \boldsymbol{e}_\theta$, which span the plane containing $\boldsymbol{t}$ and $\boldsymbol{n}$, as shown in figure 6, with $\phi(s)$ being the angle between $\boldsymbol{t}$ and $\boldsymbol{e}_\theta$. Then

$$\left.\begin{aligned} \boldsymbol{t} &= \cos\phi\boldsymbol{e}_\theta + \sin\phi\boldsymbol{n}_\theta, \\ \boldsymbol{n} &= \sin\phi\boldsymbol{e}_\theta - \cos\phi\boldsymbol{n}_\theta. \end{aligned}\right\} \tag{4.4}$$

In terms of spherical coordinates we may write $\boldsymbol{u}$ as

$$\begin{aligned}\boldsymbol{u}(s) &= \sin\beta\cos\theta\boldsymbol{e}_1 + \sin\beta\sin\theta\boldsymbol{e}_2 + \cos\beta\boldsymbol{e}_3\\ &= \sin\beta\boldsymbol{e}_\rho + \cos\beta\boldsymbol{e}_3,\end{aligned} \tag{4.5}$$

where $\boldsymbol{e}_\rho = \cos\theta\boldsymbol{e}_1 + \sin\theta\boldsymbol{e}_2$ is the radius vector in the horizontal plane containing the cylindrical frame and $\beta = \beta(s)$ and $\theta = \theta(s)$. Differentiating (4.5) yields

$$\partial_s\boldsymbol{u} = \boldsymbol{t} = \cos\beta\dot{\beta}\boldsymbol{e}_\rho + \sin\beta\dot{\theta}\boldsymbol{e}_\theta - \dot{\beta}\sin\beta\boldsymbol{e}_3 \tag{4.6}$$

in terms of the trihedron $\{\boldsymbol{e}_\rho, \boldsymbol{e}_\theta, \boldsymbol{e}_3\}$. Comparing the result with the first of relations (4.4) yields the relations

$$\dot{\theta} = \frac{\cos\phi}{\sin\beta}, \tag{4.7}$$

$$\dot{\beta} = -\sin\phi. \tag{4.8}$$

There remains the issue of describing the deformation itself in terms of the curvature of the surface. The only non-zero element of the curvature tensor for the deformation is $b_{ss} = -r\boldsymbol{n}\cdot\partial_s\boldsymbol{t}$; the other components $b_{sr} = b_{rr} = 0$. Thus, the normal curvature of the surface is

$$\frac{b_{ss}}{g_{ss}} = -\boldsymbol{n}\cdot\frac{\partial_s\boldsymbol{t}}{r} = \frac{\kappa}{r},$$

where κ is defined as the curvature of the surface at unit distance from the tip. Using (4.4), (4.7) and (4.8), we obtain the following equation for the angle ϕ:

$$\dot{\phi} = \kappa - \cot\beta\cos\phi. \tag{4.9}$$

The kinematic relations (4.7)–(4.9) are equivalent to the Frenet formulae for the geometrical description of curves (Kreyszig 1991; Struik 1988). Indeed, transposing the fundamental theorem of planar curves to our case, we assert that, once $\kappa(s)$ is known, the conical shape is completely determined by (4.7)–(4.9) up to rigid-body motions.

(*b*) *Mechanical equilibrium*

Specializing the equations of equilibrium (2.9) for the conical geometry described in the previous section, we find that

$$\partial_s\boldsymbol{F}_s + \partial_r(r\boldsymbol{F}_r) + r\boldsymbol{K} = \boldsymbol{0}, \tag{4.10}$$

$$\partial_s\boldsymbol{M}_s + \partial_r(r\boldsymbol{M}_r) + r(\boldsymbol{t}\times\boldsymbol{F}_s + \boldsymbol{u}\times\boldsymbol{F}_r) = \boldsymbol{0}. \tag{4.11}$$

These equations are closed once the constitutive relations for the torques given by (2.11) are known. Here $\boldsymbol{M}_s = B\kappa\boldsymbol{n}\times\boldsymbol{t}/r$ and $\boldsymbol{M}_r = B\sigma\kappa\boldsymbol{n}\times\boldsymbol{u}/r$.

To make further progress, we resolve the forces and torques along the orthonormal trihedron $\{\boldsymbol{t}, \boldsymbol{u}, \boldsymbol{n}\}$. Using the relations $\partial_s\boldsymbol{t} = -\kappa\boldsymbol{n} - \boldsymbol{u}$, $\partial_s\boldsymbol{u} = \boldsymbol{t}$ and $\partial_s\boldsymbol{n} = \kappa\boldsymbol{t}$, we write the force balance equation (4.10) in component form as

$$\left.\begin{aligned}\partial_s N_{ss} + \kappa Q_s = 0,\\ \partial_r(rN_{rr}) - N_{ss} = 0,\\ \partial_s Q_s + \partial_r(rQ_r) - \kappa N_{ss} - rk(s,r) = 0.\end{aligned}\right\} \tag{4.12}$$

Here we have assumed that the external force $\boldsymbol{K} = -k\boldsymbol{n}$ with $k > 0$, denoting the reaction from the cylindrical frame, i.e. we ignore any frictional interactions with the frame. Similarly, the equation for the balance of torques (4.11) can be written in component form as

$$\left.\begin{aligned} Q_s &= B\frac{\dot{\kappa}}{r^2}, \\ Q_r &= -B\frac{\kappa}{r^2}. \end{aligned}\right\} \tag{4.13}$$

We observe that equations (4.12) and (4.13) are the natural generalizations of (3.5)–(3.7) to the case of conical deformations. Substituting the expressions for the shear forces Q_s, Q_r from (4.13) into the first two equations in (4.12) and integrating, we get

$$N_{ss} = -B\left(\frac{\kappa^2}{2r^2} + \psi'(r)\right), \tag{4.14}$$

$$N_{rr} = B\left(\frac{\kappa^2}{2r^2} - \frac{\psi(r) + \varphi(s)}{r}\right), \tag{4.15}$$

where $\psi' = \mathrm{d}\psi/\mathrm{d}r$ and $\psi(r)$ and $\varphi(s)$ are two as yet unknown functions. A similar elimination of Q_r, Q_s and N_{ss} in the third equation of (4.12) yields

$$B[\ddot{\kappa} + (1 + r^2\psi'(r) + \tfrac{1}{2}\kappa^2)\kappa] = r^3 k(s, r) \tag{4.16}$$

for the curvature $\kappa(s)$. The deformed surface is perfectly conical over the region of contact, where $\kappa = \text{const}$. In the region where the surface is free, $k = 0$ so that (4.16) has a solution only when $1 + r^2\psi'(r) = a^2 = \text{const.}$, and the equation for the curvature $\kappa(s)$ is then

$$\ddot{\kappa} + (a^2 + \tfrac{1}{2}\kappa^2)\kappa = 0. \tag{4.17}$$

We note that equation (4.16) is completely analogous to (3.8) for the confined cylinder considered in § 3, but here it describes the inextensible conical deformations of an elastic sheet. Furthermore (4.17) is exactly the equation for the classical planar *Elastica*. The nature of the mathematical analogy that relates conical and cylindrical deformations of thin elastic sheets suggests the following conjecture in higher dimensions: while the kinematic constraints that describe inextensible surfaces will necessarily vary according to the dimension of the manifold and its embedding, the hypersurface which generates isometric embeddings and minimizes the squared curvature always satisfies the *Elastica* equation (4.17).

(*c*) *Global force and torque balance*

For the case of conical deformations, since $\psi'(r) = -(1 - a^2)/r^2$, we have $\psi = -(a^2 - 1)/r$.† Substituting into (4.14), (4.15), we can deduce the in-plane stresses

$$N_{ss} = -\frac{B}{2r^2}(\kappa^2 + 2(a^2 - 1)), \tag{4.18}$$

$$N_{rr} = \frac{B}{2r^2}(\kappa^2 + 2(a^2 - 1))\left(1 - \frac{r}{R_\mathrm{p}}\right). \tag{4.19}$$

† The constant of integration can be absorbed in the definition of the function $\varphi(s)$.

Here $\varphi(s)$ is determined by the boundary condition that the radial stresses vanish at the boundary of the sheet, i.e. $N_{rr}(r = R_\mathrm{p}) = 0$. As we will show later (§ 4 *g* (i)) $a^2 - 1 > 0$ for the case of moderate deflections so that the sheet is under compression in the azimuthal direction and under tension in the radial direction, i.e. $N_{ss} < 0$, $N_{rr} > 0$.

(*d*) *Forces in the contact region*

Although the solution to (4.17) yields the complete geometry of developable conical surfaces, the surfaces are not uniquely determined unless a self-equilibrated system of forces compatible with (4.16) is prescribed. Along the region of the surface in contact with the cylindrical frame, the externally applied normal force $k(s, r) = k_\mathrm{c}(r)$ must be independent of the arc length because of translational symmetry along the line $r = \text{const}$. However, this result is inconsistent with global torque balance. The torque due to the contact forces on the right side† with respect to the tip of the cone is given by

$$\boldsymbol{T}_\mathrm{right} = \int_\mathrm{right} \mathrm{d}A\, r\boldsymbol{u} \times \boldsymbol{K} = -\int_{s_\mathrm{c}}^{\pi} \mathrm{d}s\, \boldsymbol{t} \int_0^{R_\mathrm{p}} \mathrm{d}r\, r^2 k_\mathrm{c}(r). \tag{4.20}$$

In the region where the surface is in contact with the cylindrical frame, $\phi = 0$, so that $\boldsymbol{t} = \boldsymbol{e}_\theta$ and $\boldsymbol{n} = \boldsymbol{n}_\theta$. A change of variable from the arc length s to the angle θ allows us to rewrite the previous relation as

$$\boldsymbol{T}_\mathrm{right} = \sin\beta_\mathrm{c}(\sin\theta_\mathrm{c}\boldsymbol{e}_2 + (1 - \cos\theta_\mathrm{c})\boldsymbol{e}_1) \int_0^{R_\mathrm{p}} \mathrm{d}r\, r^2 k_\mathrm{c}(r). \tag{4.21}$$

A similar calculation for the contact forces on the left side gives

$$\boldsymbol{T}_\mathrm{left} = \sin\beta_\mathrm{c}(\sin\theta_\mathrm{c}\boldsymbol{e}_2 - (1 - \cos\theta_\mathrm{c})\boldsymbol{e}_1) \int_0^{R_\mathrm{p}} \mathrm{d}r\, r^2 k_\mathrm{c}(r). \tag{4.22}$$

Adding both contributions, we see that the sum does not vanish unless an additional component in the $\boldsymbol{e}_2$-direction is accounted for. Thus a localized external force is needed at the points $s = \pm s_\mathrm{c}$, where the sheet just contacts the frame. Its magnitude may be determined by requiring the balance of torques, i.e.

$$\int_{s_\mathrm{c}^-}^{s_\mathrm{c}^+} \mathrm{d}s \int_0^{R_\mathrm{p}} \mathrm{d}r\, r\boldsymbol{e}_2 \cdot (r\boldsymbol{u} \times \boldsymbol{K}) + \sin\beta_\mathrm{c} \sin\theta_\mathrm{c} \int_0^{R_\mathrm{p}} \mathrm{d}r\, r^2 k_\mathrm{c}(r) = 0, \tag{4.23}$$

where $s_\mathrm{c}^\pm = s_\mathrm{c} \pm \eta$, $\eta \to 0$. Writing the localized force at the contact points $\boldsymbol{K} = -\chi\delta(s - s_\mathrm{c})\boldsymbol{n}$, where $\delta(s)$ is the usual Dirac delta function, we find that $\chi = k_\mathrm{c} \sin\beta_\mathrm{c} \tan\theta_\mathrm{c}$ and finally

$$\boldsymbol{K} = -k_\mathrm{c}(r)(1 + \sin\beta_\mathrm{c} \tan\theta_\mathrm{c}\delta(|s| - s_\mathrm{c}))\boldsymbol{n}, \quad |s| \geqslant s_\mathrm{c}. \tag{4.24}$$

We observe that the contact force on the cone (4.24) is completely analogous to the formula for the contact forces on the puckered cylinder (3.13). Here s is the scaled length and is thus dimensionless.

† The right side is defined as the region of points with positive coordinate along the $\boldsymbol{e}_2$-direction.

(*e*) *Force at the tip*

The determination of the function $k_c(r)$ and hence the value of the total force applied at the tip can be carried out easily for the case of a conical sheet in contact with a conical frame with a constant opening angle β_c, since in this case the externally applied force is discontinuous along two radial lines $s = \pm s_c$, but not elsewhere. Evaluating (4.16) for this case gives

$$k_c(r) = B\left(a^2 + \frac{\kappa_c^2}{2}\right)\frac{\kappa_c}{r^3}, \tag{4.25}$$

where κ_c is the curvature along the contact region. Then the total external force is given by integrating (4.24) over the contact region. In the experiments to be discussed later, a flat sheet is pushed into a cylindrical frame (Cerda *et al*. 1999; Cerda & Mahadevan 1998; Chaieb & Melo 1998), leading to a localized distribution of externally applied forces along the line of contact, rather than along an area of contact. To circumvent dealing with the resulting singular distribution of external forces, we use a simpler definition for the averaged force

$$F = \frac{\partial \tilde{U}}{\partial d} = \frac{1}{R}\frac{\partial \tilde{U}}{\partial \varepsilon}, \tag{4.26}$$

where $\tilde{U}$ is the total elastic energy of the puckered sheet in contact with the cylindrical frame. Assuming that the energy of a sheet in contact with a cylindrical frame is approximately equal to the energy U of a sheet in contact with a conical frame (equivalent to an averaging procedure in the radial direction) $\tilde{U} \approx U$.

To determine the relation between the contact forces and the variation of the elastic energy, we use the principle of virtual work which states that

$$\delta U = \int_A r\,\mathrm{d}r\,\mathrm{d}s\,\boldsymbol{K}\cdot\delta\boldsymbol{r}, \tag{4.27}$$

where the domain of integration is the entire surface, A, of the cone. Because $\boldsymbol{K} = -k\boldsymbol{n}$ and is different from zero only in the contact region, the contribution to the integral arises from terms of the form $\boldsymbol{n}\cdot\delta\boldsymbol{r} = r\delta\beta_c$. Substituting for $\boldsymbol{K}$ from (4.24) into (4.27) leads to

$$\frac{\partial U}{\partial \varepsilon} = 2\sin^2\beta_c(\pi - s_c + \sin\beta_c\tan\theta_c)\int_0^{R_p}\mathrm{d}r\,r^2 k_c(r). \tag{4.28}$$

Here, the independent variable $\delta\beta_c$ has been replaced by $\delta\varepsilon$ in light of (4.1), and k_c is given by equation (4.25). Finally, in light of the geometrical identities

$$\kappa_c = \varepsilon, \qquad \sin\beta_c(\pi - \theta_c) = (\pi - s_c), \qquad \sin\beta_c = \frac{1}{(1+\varepsilon^2)^{1/2}},$$

we may write

$$F = \frac{1}{R}\frac{\partial \tilde{U}}{\partial \varepsilon} = \frac{B}{R}\ln\frac{R_p}{R_*}\frac{2\varepsilon(a^2 + \frac{1}{2}\varepsilon^2)}{(1+\varepsilon^2)^{3/2}}(\pi - \theta_c + \tan\theta_c). \tag{4.29}$$

The parameter R_* denotes the size of the core region near the tip $r = 0$, where the inextensible approximation is invalid owing to the effects of double curvature which induces stretching deformations. A detailed analysis of this region is beyond the scope of this paper; later on, we shall present a simple scaling argument for its size, consistent with earlier experiments.

(*f*) *Small-deflection analysis*

(i) *The deflection of the fold*

When $\varepsilon \ll 1$, the angle $\alpha = \frac{1}{2}\pi - \beta \sim O(\varepsilon)$, and the sheet deflection is small. Furthermore, the angle of rotation $\phi \ll 1$ and (4.8) and (4.9) show that $\dot{\alpha} \approx \phi$, so that the curvature κ yields the following differential equation for the deflection α:

$$\kappa = \ddot{\alpha} + \alpha. \tag{4.30}$$

In this limit, (4.17) for the *Elastica* reduces to

$$\ddot{\kappa} + a^2\kappa = 0. \tag{4.31}$$

To account for the possibility that the conical solution has several folds in different positions, we first solve (4.31) without choosing a specific origin for the arc-length coordinate s. If there is no contact between the angles $s_1 < s < s_2$, the general solution to (4.31) is $\kappa = A\cos a(s - s_0) + B\sin a(s - s_0)$ where s_0, the fold location is defined as $s_0 = (s_2 + s_1)/2$. The distance from s_0 to the contact point s_2 is then $s_c = s_2 - s_0$, so that $s_2 = s_0 + s_c$ and $s_1 = s_0 - s_c$. Because the sheet cannot sustain localized (point) torques in the absence of adhesive forces with the frame, the curvature is continuous at the contact points, and $\kappa(s_1) = \kappa(s_2) = \kappa_c$. Matching the solution of the free region with the perfectly conical region we find that

$$\kappa = \varepsilon\frac{\cos a(s - s_0)}{\cos as_c}. \tag{4.32}$$

The above equation defines a two-parameter family of solutions characterized by the number of folds and their amplitude, once the total deflection angle ε is given. To determine the shape of the sheet, we solve the approximate equation (4.30) and enforce continuity of the function α and its first and second derivatives at the contact points. Using $\alpha(s_1) = \alpha(s_2) = \varepsilon$ and $\dot{\alpha}(s_1) = \dot{\alpha}(s_2) = 0$ yields the solution

$$\alpha = \varepsilon\left(\frac{\sin s_c\cos a(s - s_0) - a\sin as_c\cos(s - s_0)}{\sin s_c\cos as_c - a\sin as_c\cos s_c}\right) \tag{4.33}$$

subject to the constraint of continuity of the azimuthal curvature, i.e. the second derivative, at the contact point given by

$$a\tan s_c = \tan as_c. \tag{4.34}$$

The condition (4.34) can be rewritten, by using the variable $x = as_c$, as

$$\frac{\tan s_c}{s_c} = \frac{\tan x}{x}. \tag{4.35}$$

This relation defines a single-valued function $s_c(x)$ for $0 < s_c < \pi$ (see the appendix), and defines the first condition that determines the shape of the sheet.

A second condition is given by the requirement that the surface is continuous when the arc length s varies from 0 to 2π. At the lowest order (4.7) gives

$$\dot{\theta} \approx \frac{1 - \frac{1}{2}\phi^2}{1 - \frac{1}{2}\alpha^2} \approx 1 - \tfrac{1}{2}(\alpha^2 - \dot{\alpha}^2),$$

so that this requirement may be written as $\int_{-\pi}^{\pi} \mathrm{d}s\, \dot{\theta} = 2\pi$ or

$$\int_{-\pi}^{\pi} \mathrm{d}s\, (\alpha^2 - \dot{\alpha}^2) = 0. \tag{4.36}$$

The evaluation of this integral requires knowledge of the number of folds, N, in the surface; each fold contributes

$$\begin{aligned}\int_{s_1}^{s_2} \mathrm{d}s\, (\alpha^2 - \dot{\alpha}^2) &= \varepsilon^2 \frac{s_\mathrm{c}^3 \sec^2 x - \tan s_\mathrm{c}(2x^2 - s_\mathrm{c}^2)}{s_\mathrm{c}^2 - x^2} \\ &= \varepsilon^2 I(x),\end{aligned} \tag{4.37}$$

where we have used relation (4.35) to simplify the integral, and the last relation defines the function $I(x)$. Although the angular size of the free region $s_2 - s_1 = 2s_\mathrm{c}$ can be different for each fold, here we will not consider this case, and we will assume that all folds are identical. Since the contribution from the contact regions to the integral (4.36) is $\varepsilon^2(2\pi - N \times 2s_\mathrm{c}(x))$, so that the inextensibility constraint (4.36) reads

$$g(x) \equiv 2\pi + N(I(x) - 2s_\mathrm{c}(x)) = 0. \tag{4.38}$$

Solving this last equation yields x and thence s_c via (4.34). We observe that since the inextensibility constraint is not sensitive to the position of each fold, the actual phase of the folds, s_0, remains undetermined. In § 4 *f* (iv) we will see that this phase is determined by a symmetry-breaking instability in the system.

Since it is possible to find solutions of (4.38) which have multiple folds, we must compute the energy of each solution to determine its relative stability. The bending energy stored in the deformed sheet is given by

$$U_\mathrm{b} = \tfrac{1}{2} B \ln \frac{R_\mathrm{p}}{R_*} \int_{-\pi}^{\pi} \mathrm{d}s\, \kappa^2. \tag{4.39}$$

In light of (4.30), (4.33)–(4.35) the contribution to the energy of each fold is

$$\begin{aligned}U_\mathrm{b} &= \tfrac{1}{2} B \ln \frac{R_\mathrm{p}}{R_*} \int_{s_1}^{s_2} (\ddot{\alpha} + \alpha)^2 = \tfrac{1}{2} B \ln \frac{R_\mathrm{p}}{R_*} \varepsilon^2 (\tan s_\mathrm{c} + s_\mathrm{c} \sec^2 x) \\ &\equiv \tfrac{1}{2} B \ln \frac{R_\mathrm{p}}{R_*} \varepsilon^2 e(x),\end{aligned} \tag{4.40}$$

and the total bending energy of the structure with N folds is

$$U_\mathrm{b} = \tfrac{1}{2} B \ln \frac{R_\mathrm{p}}{R_*} \varepsilon^2 (2\pi + N(e(x) - 2s_\mathrm{c}(x))). \tag{4.41}$$

(ii) *A fold with sub-folds*

For the case of a single fold, substituting $N = 1$ in equation (4.38) leads to $g(x) = 2(\pi - s_\mathrm{c}(x)) + I(x) = 0$ with a graphical solution depicted in figure 7. There is a one parameter set of solutions for this case and each corresponds to just one main fold but with a different number of sub-folds. The first root of $g(x) = 0$ is $x_1 = 4.61$ and has the profile α_1 in figure 8. For this case, the azimuthal size of the free region is

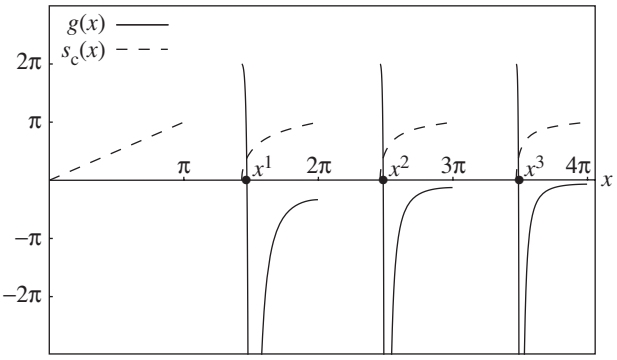

Figure 7. Graphical solution of the equation $g(x) = 2(\pi - s_c(x)) + I(x) = 0$, which defines the azimuthal size of a single fold following (4.35), (4.38).

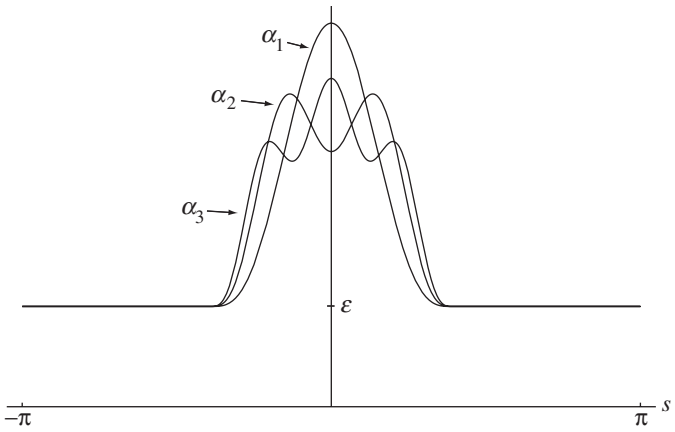

Figure 8. Angular profile $\alpha_i(s)$ corresponding to the different solutions given in table 1.

Table 1. *Energies for different configurations of one main fold*

(The solution with one sub-fold ($i = 2$) has three times more energy than the solution for no sub-fold ($i = 1$) (see figure 8).)

i	x_i	$2s_c$	$2U_b/B\ln(R/R_*)$
1	4.61	2.43	133
2	7.80	2.44	380
3	11.0	2.44	751

$2s_c = 2.43 \approx 139°$, consistent with experiment (this is the solution reported in Cerda & Mahadevan (1998)).

Continuing with this analysis, we find that the ith root of $g(x) = 0$, x_i has i sub-folds; a good approximation to its value is $x_i \approx (2i + 1)\pi/2$. However, the azimuthal extent of the free region does not change much and has an accumulation point close to $2s_c \approx 2.44$ (see table 1). To estimate the energy of these different solutions, and thence their stability, we use the expression (4.41) for the bending energy, simplified

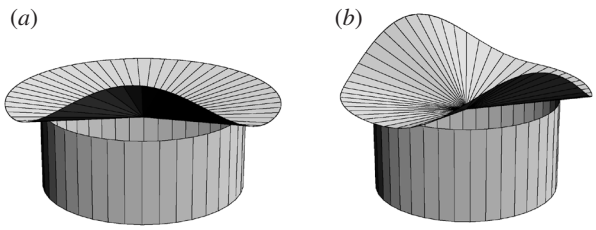

Figure 9. The conical elastica with (*a*) one fold and (*b*) two folds (see table 2).

Table 2. *Total energy of the folds given in figure 9*

N	x	$2s_c$	$2U_b/B\ln(R/R_*)$
1	4.61	2.43	133
2	4.60	2.24	169

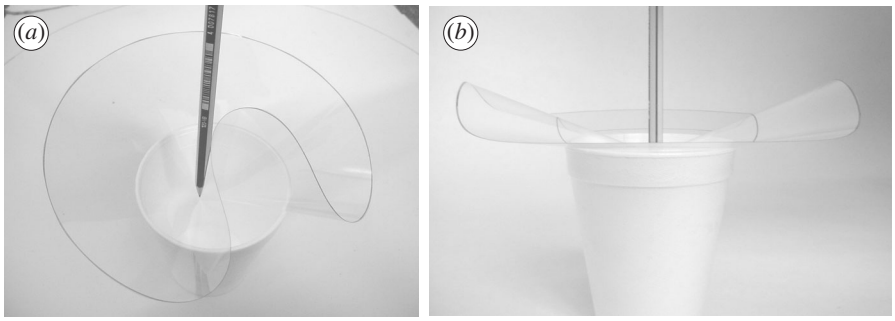

Figure 10. Photographs of a conical shape with (*a*) one fold and (*b*) two folds. The observations are consistent with our calculations, which show that the two solutions are energetically similar.

by using the inextensibility constraint so that

$$U_b = B\ln\frac{R_p}{R_*}\left[\varepsilon^2\left(\frac{x}{s_c}\right)^2(\pi+\tan s_c - s_c)\right]. \tag{4.42}$$

In table 1, we show the values of the bending energy for configurations with zero ($i = 1$), one ($i = 2$) and two ($i = 3$) sub-folds. We see that the energy for the configuration with a single sub-fold, depicted by α_2 in figure 8 is approximately three times the bending energy of the basic fold depicted by α_1, explaining why main folds with sub-folds are not observed. Because a main fold decorated with sub-folds is always energetically less favourable than one without any, from now on we will limit ourselves only to simple folds.

(iii) *Two or more folds*

We now consider the case with two or more folds. When the number of folds $N = 2$ the solution to the relation (4.38) yields $x = 4.60$, corresponding to two simple folds with an azimuthal width $2s_c = 2.24$ for each fold and is depicted in figure 9*b*, adjacent to the shape with one fold. The corresponding bending energy calculated using equation (4.41) is shown in table 2. Although the solution with

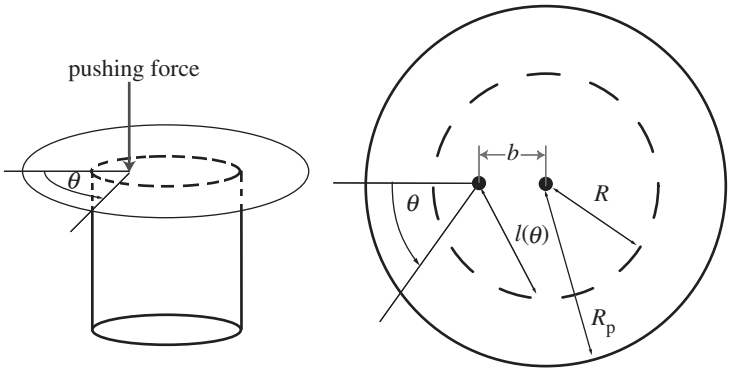

Figure 11. Schematic of set-up and geometry when the packing force is applied at a distance b from the centre of the frame.

one fold is energetically preferred, the relative energy difference $(U_{\mathrm{b}}[\text{two folds}] - U_{\mathrm{b}}[\text{one fold}])/U_{\mathrm{b}}[\text{one fold}] \approx 0.3$ is not so big. Indeed, it is possible to observe the solution with two folds (see figure 10) when some care is taken.

For the case $N = 3$ the relation (4.38) yields $x = 4.58$ but this solution is inadmissible because the total angular sector over which the sheet is in contact with the cylinder is $(2\pi - 3 \times 2s_{\mathrm{c}}) < 0$. This conclusion is also qualitatively consistent with our observations.

(iv) *Determination of the phase and position of a fold*

We now consider the azimuthal location of the fold. If the sheet is pushed axisymmetrically at the centre of the frame, the position of the fold is undetermined and s_0 is unknown. This symmetry is broken if the force is applied at a distance b from the centre, as shown in figure 11. Then the angle α that the generators make with the horizontal plane must satisfy the inequality

$$\alpha \geqslant \varepsilon(\theta), \tag{4.43}$$

where $\varepsilon(\theta) = d/\ell(\theta)$, with $\ell(\theta) = -b\cos\theta + (R^2 - b^2\sin^2\theta)^{1/2}$ being the distance from the point of application of the force to the cylindrical frame and the angle θ as measured in figure 11. In terms of the two dimensionless parameters, $\varepsilon = d/R$ and $\delta = b/R$, we can write

$$\varepsilon(\theta) = \frac{\varepsilon}{-\delta\cos\theta + (1 - \delta^2\sin^2\theta)^{1/2}}. \tag{4.44}$$

Since the relations (4.30), (4.31) remain valid in this regime, the shape of the sheet in the free region can be written as

$$\alpha = A\cos a(s - s_0) + B\cos(s - s_0) + C\sin a(s - s_0) + D\sin(s - s_0). \tag{4.45}$$

However, the continuity conditions at the point of contact with the frame are now different from the earlier case where the sheet is pushed symmetrically. To leading order, $s \approx \theta$, so that continuity of the deflection $\alpha(s)$ and its derivative

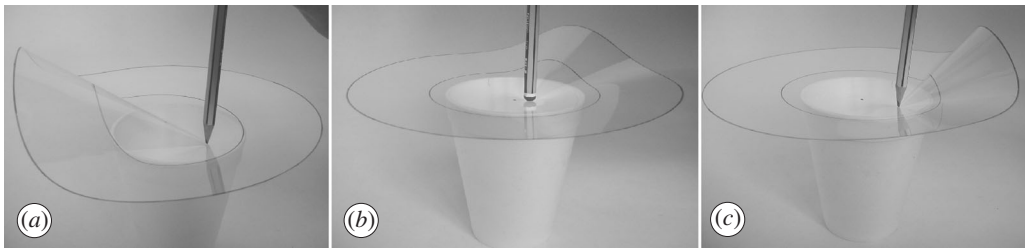

Figure 12. The photographs show a fold at (*a*) π, (*b*) $\pi/2$ ($-\pi/2$ corresponds to a reflection about an axis connecting the centre of the circle to the point of forcing) and (*c*) 0.

yields $\alpha(s_1) = \varepsilon(s_1)$ and $\dot{\alpha}(s_1) = \dot{\varepsilon}(s_1)$, etc. Therefore,

$$\begin{aligned}\alpha = \frac{1}{2W_1}[&((\varepsilon_2+\varepsilon_1)\sin s_c + (\dot{\varepsilon}_2-\dot{\varepsilon}_1)\cos s_c)\cos a(s-s_0)\\ &- ((\dot{\varepsilon}_2-\dot{\varepsilon}_1)\cos as_c + (\varepsilon_2+\varepsilon_1)a\sin as_c)\cos(s-s_0)]\\ &+ \frac{1}{2W_2}[((\varepsilon_2-\varepsilon_1)\cos s_c - (\dot{\varepsilon}_2+\dot{\varepsilon}_1)\sin s_c)\sin a(s-s_0)\\ &+ ((\dot{\varepsilon}_2+\dot{\varepsilon}_1)\sin as_c - (\varepsilon_2-\varepsilon_1)a\cos as_c)\sin(s-s_0)],\end{aligned} \tag{4.46}$$

where $\varepsilon_1 = \varepsilon(s_1)$ and $\dot{\varepsilon}_1 = \dot{\varepsilon}(s_1)$, etc., and

$$W_1 = (\sin s_c \cos as_c - a\sin as_c \cos s_c), \qquad W_2 = (\sin as_c \cos s_c - a\sin s_c \cos as_c).$$

The continuity of the second derivative (azimuthal curvature)

$$\ddot{\alpha}(s_1) = \ddot{\varepsilon}(s_1), \qquad \ddot{\alpha}(s_2) = \ddot{\varepsilon}(s_2) \tag{4.47}$$

gives

$$\left.\begin{aligned}\ddot{\alpha}(s_2) + \ddot{\alpha}(s_1) &= \ddot{\varepsilon}(s_2) + \ddot{\varepsilon}(s_1),\\ \ddot{\alpha}(s_2) - \ddot{\alpha}(s_1) &= \ddot{\varepsilon}(s_2) - \ddot{\varepsilon}(s_1).\end{aligned}\right\} \tag{4.48}$$

These two conditions together with the inextensibility constraint (4.36) are sufficient to determine the contact parameters a, s_c and s_0.

We are now ready to consider the limit $\delta \ll 1$ and determine the phase of the fold. In this limit the conditions (4.47) yield $\ddot{\varepsilon}(s) \approx 0$ and $\ddot{\alpha}(s_2) \approx \ddot{\alpha}(s_1) \approx 0$, so that (4.47) is equivalent to (4.35) studied for the axisymmetric case in § 4 *f* (i). However, the second condition in (4.48) does not have a corresponding limit and an expansion of this equation to second order gives

$$\begin{aligned}(2\sin s_c \sin s_0)\varepsilon\delta + \left(\frac{(a^2-1)\sin^2 s_c \sin as_c}{W_2} + \cos s_c\right)\sin s_c \sin 2s_0 \varepsilon\delta^2 + O(\delta^3)\\ = (2\sin s_c \sin s_0)\varepsilon\delta + 4\sin s_c \cos s_c \sin 2s_0 \varepsilon\delta^2 + O(\delta^3).\end{aligned}$$

As $\delta \to 0$, the above equation has the approximate solution $\sin 2s_0 = 0$, so that the phase of the fold $s_0 = 0, \pm\pi/2, \pi$, and can be verified for arbitrary δ using a more sophisticated calculation. By pushing a sheet of acetate into a cylinder with small variations in the centre of force, it is easy to observe that the fold will be in one of these positions, as shown in figure 12.

(*g*) *Large-deflection analysis*

To understand the onset of nonlinear behaviour, we consider the force–displacement response of the system. We start with (4.29), which yields $F \sim \varepsilon$ when $\varepsilon \ll 1$, i.e. the system behaves like a linear spring for small deformations. Using the linear solution obtained in (4.32), we find that the curvature amplitude is $\varepsilon/\cos as_c$ with $\cos as_c = \cos x \approx -0.1$ for the solution with one fold ($x \approx 4.61 \approx 3\pi/2$ in table 2). Therefore, we expect nonlinear behaviour when the maximum curvature is no longer small, i.e. when $\varepsilon \approx 0.1$.

(i) *Determination of the displacement*

The set of angles $\{\theta, \beta, \phi\}$ that determine the shape of the developable cone corresponds to the classical Euler angles for the kinematics of rigid-body motion. While this allows us to study the large deformation behaviour of sheets, this representation breaks down at the polar singularities $\beta = 0, \pi$. To describe arbitrary rotations, we resort to the use of a singularity-free parametrization of rotations in terms of the Euler parameters q_0, q_1, q_2, q_3 (which are the components of the quaternions of Hamilton) recalling that the Euler angles are related to the Euler parameters via the relations (Goldstein 1980)

$$\left.\begin{aligned} q_0 &= \cos\tfrac{1}{2}\beta\cos\tfrac{1}{2}(\theta+\phi), & q_2 &= \sin\tfrac{1}{2}\beta\sin\tfrac{1}{2}(\theta-\phi),\\ q_1 &= \sin\tfrac{1}{2}\beta\cos\tfrac{1}{2}(\theta-\phi), & q_3 &= \cos\tfrac{1}{2}\beta\sin\tfrac{1}{2}(\theta+\phi). \end{aligned}\right\} \tag{4.49}$$

Once the curvature of the conical surface is determined by solving (4.16), the shape of the surface is reduced to the integration of the kinematic relations (4.7)–(4.9). In terms of the Euler parameters, these nonlinear equations acquire extraordinary simplicity and yield the linear system

$$\left.\begin{aligned} \dot{q}_0 &= -\tfrac{1}{2}(\kappa q_3 + q_2), & \dot{q}_2 &= -\tfrac{1}{2}(\kappa q_1 - q_0),\\ \dot{q}_1 &= \tfrac{1}{2}(\kappa q_2 - q_3), & \dot{q}_3 &= \tfrac{1}{2}(\kappa q_0 + q_1). \end{aligned}\right\} \tag{4.50}$$

In the contact region the integration is accomplished trivially since the curvature is constant. Then $\theta = \pi - (\pi - s)/\sin\beta_c$, $\beta = \beta_c$ and $\phi = 0$ with $\beta_c(\varepsilon)$ given by relation (4.1), and immediately yields the values of the quaternions in terms of (4.49) there. In the free region, equations (4.17) and (4.50) for the free *Elastica* are coupled and must be integrated simultaneously for $0 < s < s_c$ with the boundary conditions $\beta(s_c) = \beta_c$, $\theta(s_c) = \theta_c$, $\phi(s_c) = 0$ and $\kappa(s_c) = \varepsilon$, $\theta(0) = 0$, $\phi(0) = 0$ and $\dot{\kappa}(0) = 0$ (the symmetry of the solution ensures that the curvature is an even function of the arc length, so that its derivative is zero in the plane of symmetry). The five unknowns: β, θ, ϕ, κ and $\dot{\kappa}$, and the unknown parameters s_c and a^2 can then be found using a shooting method to solve (4.50) in light of the seven boundary conditions.

Figure 13*a* shows the arc length s_c and the angle of contact θ_c as a function of the parameter ε. We observe that s_c and θ_c are similar when $\varepsilon \leqslant 0.1$ as expected, but diverge for larger values of ε. Our analysis of the forces in § 4 *d* showed that the contact angle $\theta_c < \pi/2$ in the absence of any adhesive contact forces. This limits the validity of our analysis to situations where $\varepsilon \approx 0.97$ or $\beta_c \approx 46^\circ$. Beyond this the conical structure is unstable, and in a displacement-controlled experiment the

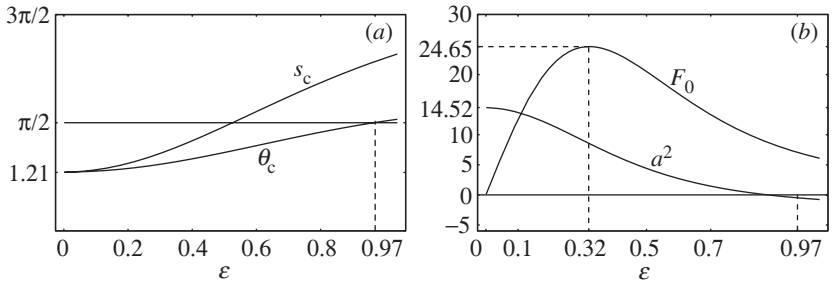

Figure 13. (*a*) Numerical values of the contact arc length s_c and its projection θ_c as a function of the vertical displacement ε. (*b*) The dimensionless force F_0 and the Lagrange parameter a^2 as a function of ε. These solutions were obtained by solving (4.17), (4.50).

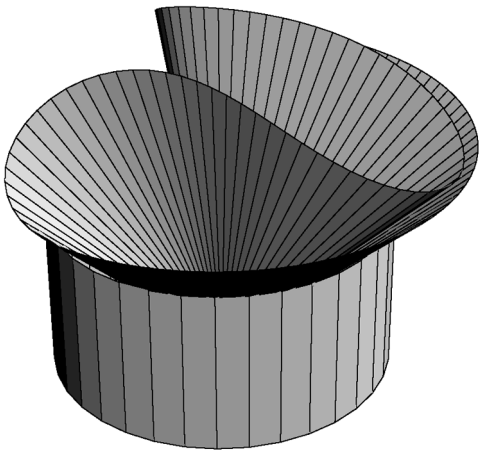

Figure 14. Geometry of the conical solution for the value $\varepsilon \approx 0.97$.
The structure collapses when $\varepsilon > 0.97$ in a displacement-controlled experiment.

conical shape will collapse on itself with new regions of contact to balance torques globally. Figure 14 shows the shape of the surface for this limiting value of ε.

To understand the response of the sheet to a force, in figure 13*b* we plot the dimensionless axial force $F_0 = RF/B\ln(R_p/R_*)$ and the Lagrange multiplier $a^2(\varepsilon)$, which is a measure of the azimuthal force as a function of the packing parameter ε. We observe the expected linear relation $F_0 \sim \varepsilon$ and $a^2 \sim$ const. for $\varepsilon \ll 1$. Since $a^2 \sim$ const. the azimuthal force $N_{ss} = -B(a^2-1)/r^2 < 0$ (see equation (4.18)), as expected. As ε is increased, a^2 and thence N_{ss} decrease monotonically, and can switch sign, eventually becoming tensile for $\varepsilon \sim 0.97$. A second consequence is that the total force F_0, which depends on a^2, as seen in (4.29), is a non-monotonic function of ε and has a maximum when $\varepsilon \approx 0.32$; hence the structure will collapse in a force-controlled experiment when $F \geqslant F_0(\varepsilon \approx 0.32) \approx 24.65$. The physical mechanism driving this instability can be seen most easily by considering its two-dimensional analogue, which arises when a thin plate is pushed in between two supports by a force that acts normal to the line joining the supports. In the absence of friction, the reactions from the supports gradually rotate towards each other until they can no longer balance the applied force, leading to a collapse of the structure.

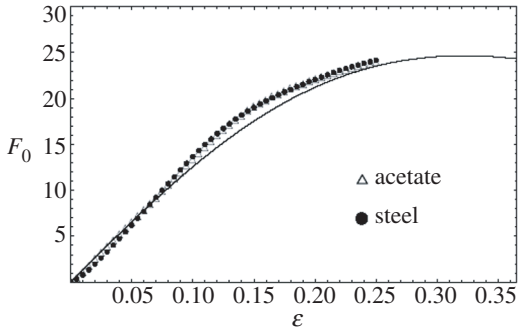

Figure 15. Experiments for two sheets of different materials. We plot the dimensionless force $F_0 = RF/B\ln(R/R_*)$ after fitting the linear part by using the parameter R_*. For acetate $B = 5.1 \times 10^{-4}$ N m, $R = 1.0 \times 10^{-2}$ m and $R_\mathrm{p} = 1.5 \times 10^{-2}$ m, so that the size of the core is found as $R_* = 3.4$ mm. For steel, $B = 7.8 \times 10^{-3}$ N m, $R = 3.8 \times 10^{-2}$ m and $R_\mathrm{p} = 4.3 \times 10^{-2}$ m and then the size of the core is $R_* = 3.6$ mm.

(ii) *Comparison with experiment*

We now turn to a comparison of our results with experiments on the response of a conically deformed sheet (Chaieb & Melo 1998; Cerda *et al*. 1999) that is packed into a cylindrical frame. In figure 15 the response curve showing the force F versus the displacement $\varepsilon \in (0, 0.2)$ is given for sheets of acetate and steel.

Since the axial force given by equation (4.29) is a universal function of the deflection ε except for a factor

$$\frac{B}{R}\ln\left(\frac{R_\mathrm{p}}{R_*}\right)$$

(see equation 4.29), we expect all the experimental data to collapse onto this curve. In figure 15 we show that this is indeed true. We note that the data collapse requires fitting the linear regime to determine the size of the core R_*, which we verify to be consistent with the experimentally measured values; the bending stiffness B, the diameter of the cylinder R and the plate radius R_p are all independently measured. Furthermore, the curves show that the linear relation between force and deformation persists for $\varepsilon \leqslant 0.1$, beyond which the sheet responds by softening nonlinearly, consistent with our theoretical estimates.

This softening behaviour has a simple geometric origin. In the absence of friction, the contact forces from the confining container are always normal to the sheet. Thus as the deformation increases, these forces rotate and eventually cannot sustain the sheet in equilibrium. This leads to a geometric instability in a force-controlled experiment—one that saturates when different parts of the sheet come into contact.

(iii) *The size of the core*

We now estimate the core size characterized by the radius R_*, which results from a balance between the bending and stretching energy. In the core of area ΔS, the stretching energy is $U_\mathrm{s} \sim E_\mathrm{s}\gamma^2\Delta S$, where γ is the in-plane strain and E_s is the stretching stiffness. The bending energy in the core is $U_\mathrm{b} \sim E_\mathrm{b}\kappa^2\Delta S$, where κ is the mean curvature in the core and characterizes the bending strain and E_b is the bending stiffness of the sheet ($=B$ for the case of an isotropic sheet). When $\alpha, \alpha' \ll 1$,

$U_\mathrm{b} \sim \kappa^2 \sim \alpha^2 \sim \varepsilon^2$. Therefore, for small deformations, $\kappa \sim \varepsilon/R_*$. The stretching strain can be estimated from the change in length of a typical generator of length R (corresponding to the size of the cylinder), the scale over which forces and torques are exerted. Due to the stretching induced by bending in the core region the length of the generator becomes $\sqrt{R^2 + \varepsilon^2 R_*^2}$; this leads to a stretching strain of order

$$\gamma \sim \left(\frac{\sqrt{R^2 + \varepsilon^2 R_*^2} - R}{R} \right) \sim \left(\frac{\varepsilon R_*}{R} \right)^2.$$

Substituting these strains into the expression for the total energy leads to

$$U \sim U_\mathrm{b} + U_\mathrm{s} \sim \left(E_\mathrm{b} \frac{\varepsilon^2}{R_*^2} + E_\mathrm{s} \frac{\varepsilon^4 R_*^4}{R^2} \right) \Delta S. \tag{4.51}$$

We note that this energy increases when R_* is too big or too small, so that there is a natural optimum size of the core for a given displacement ε. Minimizing U in (4.51) with respect to R_* yields the scaling law

$$R_* \sim \left(\frac{E_\mathrm{b}}{E_\mathrm{s}} \right)^{1/6} \varepsilon^{-1/3} R^{2/3}, \quad \varepsilon \ll 1, \tag{4.52}$$

consistent with our prior experimental results (Cerda *et al.* 1999). The first factor in the scaling law is associated with material properties; for an isotropic material,

$$\frac{E_\mathrm{b}}{E_\mathrm{s}} \sim \frac{h^2}{1 - \nu^2},$$

where h is the sheet thickness and ν is Poisson's ratio. The second arises from the geometry of deformation since ε characterizes the cone angle. This factor also hides a subtle dependence on the force

$$F = \frac{1}{R} \frac{\partial U_\mathrm{b}}{\partial \varepsilon}$$

since the force–deflection relation, discussed earlier, is of the form

$$\varepsilon = v\left(\frac{FR}{E_\mathrm{b}} \right),$$

where $v(s)$ is a dimensionless function. There is also a logarithmic dependence on the sheet radius R_p. The third factor characterizes the length R associated with the moment arm of the reaction force along the hoop. We note that this scaling law is valid for contact with a cylindrical edge where the forces and torques are applied over a length R much larger than the core size $R_* \ll R$ so that the sheet responds to stretching only very gently in response to the constraint of packing. If, on the other hand, the sheet is packed into a perfect cone, it will come into contact with this enveloping cone everywhere except in the core region. Then $R \sim R_*$, so that the scaling law (4.52) is modified to

$$R_* \sim \left(\frac{E_\mathrm{b}}{E_\mathrm{s}} \right)^{1/2} \varepsilon^{-1}$$

(Ben Amar & Pomeau 1997; Cerda & Mahadevan 1998).

In Cerda *et al.* (1999), when $\varepsilon \geqslant 0.1$, we reported a second scaling law. However, this claim is not borne out under further scrutiny, and evidence for this comes from the fact that the force–displacement curve does not show any scaling behaviour for moderate/large ε.

5. Discussion

The packing of continua generally involves a number of features:

(i) a reduction in the available area or volume that is main cause of packing;

(ii) the presence of regions of contact of the sheet, either with itself or with the confining boundary;

(iii) a small number of constituent 'elements' that interact with each other to produce a structure with a distribution of length-scales;

(iv) the presence of nearly singular structures such as contact lines and peaks;

(v) disorder in the distribution of the inhomogeneities and structures.

In both problems studied we used a combination of exact solutions and dimensional reasoning to analyse some of these features; the strong geometrical similarity between the two problems allowed us to treat them in a unified way. Our treatment has, however, been limited to answering only the simplest of questions associated with the shape, response and stability of the 'elementary excitations' in these packing problems in the limit of weak to moderate confinement. As the confinement becomes strong, the number of these 'excitations' increases and they interact with each other to form higher-order structures on a range of length-scales. The difficult question of how the topological constraint of impenetrability is manifested in the physical realization of crumpling is one which we have not addressed here. However, this is clearly one of the defining characteristics of strongly crumpled sheets, and has, to the authors' knowledge, never been treated in a systematic way.

We conclude with a discussion of how our results might shed light on the question of crumpling and packing of continua. It might be easier to treat the case of cylindrical packing, since we know that the shape of the cross-section of the multilobed cylindrical sheet must be made up of circular arcs (where it is in contact with the confining cylinder), elliptic functions (solutions to the *Elastica* equation) and flat regions (where different parts of the sheet are in contact with each other in the interior of the cylinder). In the packed sheet, these elementary 'excitations' must be glued together along contact lines where the curvature of the sheet is continuous but its tangential derivative suffers a jump proportional to the normal force between the sheet and itself and/or the confining boundary, as we have already seen in the analysis of a single 'bump' in the puckered cylinder.

In the case of true three-dimensional packing and crumpling, our study has uncovered the role of geometric instabilities that lead to the generation of smaller and smaller length-scales. A series of such events, i.e. geometric softening, dynamic snap-through, local topological stiffening, provides us with a microscopic mechanism for the crumpling of a large thin elastic sheet. As the sheet is deformed by a force, it forms a developable cone that deforms, softens and eventually becomes dynamically

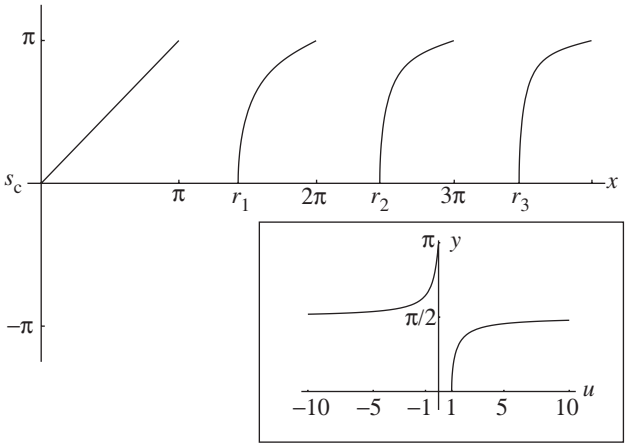

Figure 16. A plot of the function $s_c(x)$.

unstable, and an acoustic pulse is emitted when the sheet pops into a folded configuration. This stiffens the sheet locally, but soon new developable cones and stretched ridges which connect them begin to form. Ridges may buckle in the plane of the ridge by forming a developable cone about which the ridge pivots and folds, locally leading to roughly the same scenario as that for a single conical dislocation, or they may buckle in a direction perpendicular to the ridge by forming two dislocations that move apart along a new ridge about which the original ridge folds, leading to a scenario like that seen during the bending of a drinking straw. This second scenario stiffens the sheet enormously by forming a convex cylindrical structure. A cascade of these instabilities on ever decreasing length-scales leads to the formation of new conical dislocations as the sheet crumples, and the energy of deformation is pumped down to smaller and smaller scales. As the size of these folds becomes smaller, the incremental deformation is concomitantly less, and a cross-over to the regime where stretching and bending deformations are of the same order is likely. However, any analysis of this stage in crumpling must also account for inelastic deformations. On length-scales much larger than the thickness but much smaller than the length or breadth of the sheet, these dynamical snap-throughs could constitute a self-similar cascade. This is an area that could quite clearly benefit from further computational, theoretical and experimental work.

E.C. acknowledges the support of a Fundación Andes Postdoctoral Fellowship 2001, Universidad de Santiago DICYT project 'The tablecloth problem' (1999–2001), Fondecyt 1020359 (2002) and Fondap 11980002 (2002). L.M. acknowledges the support of ENS-Paris through the Chaire Condorcet (2001), ESPCI-Paris through the Chaire Paris Sciences (2001), the US Office of Naval Research Young Investigator Program and the Schlumberger Chair Fund (University of Cambridge, UK).

Appendix A. Definition of the function $s_c(x)$

Relation (4.35) can be written as

$$s_c(x) = y\left(\frac{\tan x}{x}\right) \tag{A 1}$$

and defines $s_c(x)$. For the function $u(y) = \tan y/y$ in the interval $0 < y < \pi$, we find that $\tan y/y > 1$ or $\tan y/y < 0$ so that the inverse function $y(u)$ is undefined in $0 < u < 1$ (see inset in figure 16).

The non-existence of the function $y(u)$ for a range of values of u implies that $s_c(x)$ does not exist for a range of x determined by $0 < \tan x/x < 1$, i.e. when $x \in [n\pi, r_n]$, $n = 1, 2 \ldots$, where r_n is the positive root of the equation $\tan x = x$ when $n\pi < x < (1 + n)\pi$. For instance, $r_1 = 4.49$, $r_2 = 7.72$, etc. In figure 16 we show the particular form of $s_c(x)$ which determines the shape of the sheet with one or two folds.

References

Antman, S. 1993 *Nonlinear problems of elasticity*. Springer.

Ben Amar, M. & Pomeau, Y. 1997 Crumpled paper. *Proc. R. Soc. A* **453**, 729–755.

Cerda, E. & Mahadevan, L. 1998 Conical surfaces and crescent singularities in crumpled sheets. *Phys. Rev. Lett.* **80**, 2358–2361.

Cerda, E., Chaieb, S., Melo, F. & Mahadevan, L. 1999 Conical dislocations in crumpling. *Nature* **401**, 46–50.

Chaieb, S. & Melo, F. 1998 Experimental study of developable cones. *Phys. Rev. Lett.* **80**, 2354–2357.

Dym, C. L. 1990 *Theory of shells*. New York: Hemisphere.

Goldstein, H. 1980 *Classical mechanics*. Addison-Wesley.

Kreyszig, E. 1991 *Differential geometry*. New York: Dover.

Landau, L. D. & Lifshitz, E. M. 1997 *Theory of elasticity*, 3rd edn. London: Butterworth-Heinemann.

Lobkovsky, A., Gentges, S., Li, H., Morse, D. & Witten, T. 1995 Stretched ridges in crumpling. *Science* **270**, 1482–1485.

Love, A. E. H. 1944 *A treatise on the mathematical theory of elasticity*. New York: Dover.

Mallock, A. 1908 Note on the instability of tubes subjected to end pressure, and on the folds in a flexible material. *Proc. R. Soc. A* **81**, 388–393.

Rayleigh, Lord 1922 *Theory of sound*, vol. 1, ch. Xa. New York: Dover.

Reissner, E. 1941 A new derivation of the equations for the deformation of elastic shells. *Am. J. Math.* **63**, 177–184.

Struik, D. J. 1988 *Lectures on classical differential geometry*. New York: Dover.

Witten, T. & Li, H. 1993 Asymptotic shape of a fullerene ball. *Europhys. Lett.* **23**, 51–58.

As this paper exceeds the maximum length normally permitted,
the authors have agreed to contribute to production costs.